Photoneutron cross sections of ^{58}Ni and ^{60}Ni[‡]

S. C. Fultz,[†] R. A. Alvarez, B. L. Berman, and P. Meyer

Lawrence Livermore Laboratory, University of California, Livermore, California 94550

(Received 10 January 1974)

Photoneutron cross sections of ^{58}Ni and ^{60}Ni have been measured, using separated isotopes and nearly monoenergetic photons from in-flight annihilation of positrons. Both (γ, n) and $(\gamma, 2n)$ cross sections have been obtained; the $(\gamma, 3n)$ cross section for both isotopes was found to be essentially negligible up to the highest energy measured, 33.5 MeV. The peak cross section of 27 mb for ^{58}Ni occurs at 17.3 MeV, while for ^{60}Ni the peak cross section of 74 mb occurs at 16.3 MeV. The $(\gamma, 2n)$ cross section of ^{58}Ni is small, never exceeding 1.5 mb, whereas in the case of ^{60}Ni the $(\gamma, 2n)$ cross section rises to a peak value of just over 10 mb at approximately 24 MeV, where it constitutes over 30% of the total photoneutron cross section. In both nuclei the $(\gamma, 2n)$ cross section appears essentially to vanish above 33 MeV, whereas the single-neutron cross sections of both appear to remain nearly constant from about 25 MeV to the maximum measured energy. Considerable structure appears in the total cross section of both nuclei throughout the giant-resonance region. Structure is also evident in the $(\gamma, 2n)$ cross sections, particularly in the case of ^{60}Ni. Integrated total photoneutron cross sections up to 33.5 MeV were determined to be 286 MeV mb for ^{58}Ni and 704 MeV mb for ^{60}Ni. Our results are compared with those from previous photoneutron experiments, and, combined with measured photoproton cross sections, are used to test theoretical predictions based on shell-model calculations.

NUCLEAR REACTIONS ^{58,60}Ni(γ, n), $(\gamma, 2n)$, $E = 12$–34 MeV; measured $\sigma(E)$; deduced integrated cross sections, symmetry energies. Enriched targets, monoenergetic photons, resolution 75–160 keV.

I. INTRODUCTION

Photonuclear reactions in ^{58}Ni and ^{60}Ni are particularly interesting both because of the structure that appears to exist in the region of the giant resonance and because of the greatly different magnitudes of their photoneutron cross sections. The latter effect, together with the associated differences in their photoproton cross sections, indicates that isotopic spin probably plays an important role in the $E1$ photon absorption process, and the gross structure in the nickel cross sections has been interpreted by some authors[1,2] in terms of isospin splitting of the giant resonance. Owen, Muirhead, and Spicer[3] interpret the structure in terms of the collective correlations model.[4]

The present set of measurements constitutes an effort to determine, with fairly high resolution, the magnitudes of the photoneutron cross sections and the structure of the giant resonance in the ^{58}Ni and ^{60}Ni isotopes using nearly monoenergetic photons from in-flight annihilation of positrons produced by the new Livermore electron-positron linear accelerator. In addition to being the first measurements on the separated nickel isotopes with monoenergetic photons, these are the first data for which the $(\gamma, 2n)$ cross sections actually have been measured.

Previous photoneutron experiments with separated-isotope targets have been performed by Min and White[5] with rather coarse resolution. Measurements with somewhat better resolution have been made by Goryachev et al.[6] and by Owen, Muirhead, and Spicer.[3] Photoproton cross sections of ^{58}Ni and ^{60}Ni have been measured by Ishkhanov et al.[7] and by Shoda and collaborators,[8] and the ^{60}Ni (γ, p_0) cross section has been determined with high resolution by Diener et al.[1] from ^{59}Co$(p, \gamma_0)^{60}$Ni measurements. The giant resonance in the nickel isotopes also has been studied with inelastic electron scattering by Gul'karov et al.[9] Activation techniques, with bremsstrahlung, have been used to obtain (γ, n) and (γ, p) cross sections for ^{58}Ni from natural-nickel samples by Katz et al.[10] and by Carver and Turchinetz.[11] Bremsstrahlung measurements of photonuclear processes in natural nickel have also been made.[12]

II. EXPERIMENTAL METHOD

The experimental method employed in the present measurements was similar to that used in a number of earlier experiments by the Livermore photonuclear group and described in detail previously.[13] Briefly, the method consists of using a positron beam incident upon a low-Z target to

produce photons by annihilation in flight. The nar-
rowly collimated forward-going photons, owing to
the nature of the relativistic two-body kinematics
of the annihilation process, have a nearly unique
energy which depends only upon the energy of the
incident positrons. The collimated photon beam
passes through a xenon-filled spherical ion cham-
ber, which serves as a flux monitor, and impinges
on the photoneutron sample under study (held in a
low-mass Styrofoam container) located at the cen-
ter of a high-efficiency neutron detector. The
annihilation photons are, of course, accompanied
by a continuous spectrum of photons from positron
bremsstrahlung produced in the annihilation tar-
get. The contribution to the neutron yield due to
the latter (which is a smooth function of energy)
is measured on a separate set of runs with inci-
dent electrons, and subtracted out. Sample-out
backgrounds also were obtained from another set
of runs and taken into account in reducing the data.
The essential experimental differences between
the present measurement and the earlier Liver-
more measurements lie in the production and
transport of the positron beam and in the use of
an on-line computer to collect, sort, and record
the data.

The source of positrons for this experiment was
the new Livermore electron-positron linear ac-
celerator which consists of a high-current gun,
a buncher, and five S-band traveling wave ac-
celerator sections which provide a fully-loaded
energy gain of approximately 15 MeV per section.
High-Z converter targets, in which positrons are
produced, can be inserted at the end of either the
first, third, or fourth accelerator sections. The
bulk of the nickel data were taken with positrons
from the first converter.

The positrons, after having been accelerated to
the appropriate energy in the remaining sections
of the linac, pass through an achromatic beam-
transport system consisting of two $22\frac{1}{2}°$ bending
magnets (separated by energy-defining slits) and
a number of quadrupoles, and are finally focused
onto the annihilation target by a second set of
bending magnets and quadrupoles. A plan view
of the beam transport system and experimental
apparatus is shown in Fig. 1; the inset figure
shows the experimental apparatus, in elevation
view, in greater detail. Not shown in the figure
are several additional magnets in the beam trans-
port system which can bend the beam into other
experimental areas.

In the present experiment the annihilation target
was a disk of beryllium of 1.3 cm diam with a
thickness of 0.013 cm. Typically the positron
beam diameter was such that over 90% of the beam
passed through a retractable 0.95-cm-diam colli-
mator located just upstream from the annihilation
target. This collimator was used as a tuning aid
only, and was withdrawn during data runs. After
traversing the annihilation target the residual
positron beam was swept through a 90° bend and
dumped in a 5-m-deep hole. The forward-going
photons were collimated to a circular beam with a
half-angle of 7.24 mrad. The nickel target sam-
ples were 0.64-cm-thick metal disks, 3.8 cm in
diameter with masses of 61.92 g for ^{58}Ni and
65.21 g for ^{60}Ni, and were located at a distance
of 310 cm from the annihilation target; the sample
enrichments were 99.89 and 99.79%, respectively.

The flux of photons was determined for each run
from the charge collected by the ion chamber.
The energy-dependent calibration of the ion cham-
ber is known from a separate series of measure-
ments performed with greatly reduced beam cur-
rent in which the charge on the ion chamber was
measured simultaneously with the counting of
annihilation photons in a 20×20-cm cylindrical
NaI(Tl) crystal located behind the neutron detector,
as shown in Fig. 1. The ion-chamber calibration
has been determined to be independent of beam
intensity over the range encompassing both the
calibration measurements and normal data-taking
intensities.

The neutron detector consists of a 61-cm cube
of paraffin moderator in which are embedded 48
51-cm-long BF_3 detectors. The latter are ar-
ranged in an array of four coaxial rings, each
containing 12 tubes, cylindrically symmetric
about the beam line. A 7.6-cm-diam through hole
is provided for the beam, and the target sample
is positioned at the center. For each annihilation-
photon energy the number of neutron counts in
each ring is measured, which provides not only
the raw counting rates necessary for computing
the cross sections but also the average neutron
energy which is determined by the ratio of counts
in the outer and inner rings of BF_3 tubes (the
"ring ratio"). Since the ring ratios and efficiencies
of the detector have been measured previously as
a function of neutron energy using a variety of
neutron sources, the ring ratios obtained during
each photoneutron experiment provide the basis
of a point-by-point knowledge of the detector ef-
ficiency. Over the energy range of the present
measurements the detector efficiency varied be-
tween 29 and 49%. The constancy of the detector
efficiency with time was checked during these
runs by periodically inserting a calibrated neutron
source. Further details of the detector, and in
particular its efficiency calibration, are given in
previous publications.[13]

During each data run the counts from each ring
of BF_3 tubes in the detector were fed into the on-

line computer during a 300-μsec gate which was opened after each beam pulse. The start of the gate occurred about 6 μsec after the beam pulse. This delay was necessary in order to avoid counts from the gamma-flash, and the small effect on the detector efficiency has been taken into account in the data-reduction procedure. The computer recorded the number of events in which one, two, three, etc., neutrons were detected within the gate and the ring distribution for each category of event. Thus ring ratios, and therefore the detector efficiency, could be separately determined for two-neutron as well as single-neutron events. A statistical analysis of the multiplicity counts gave information on the $(\gamma, 2n)$ cross sections as well as the (γ, n) cross sections. Of
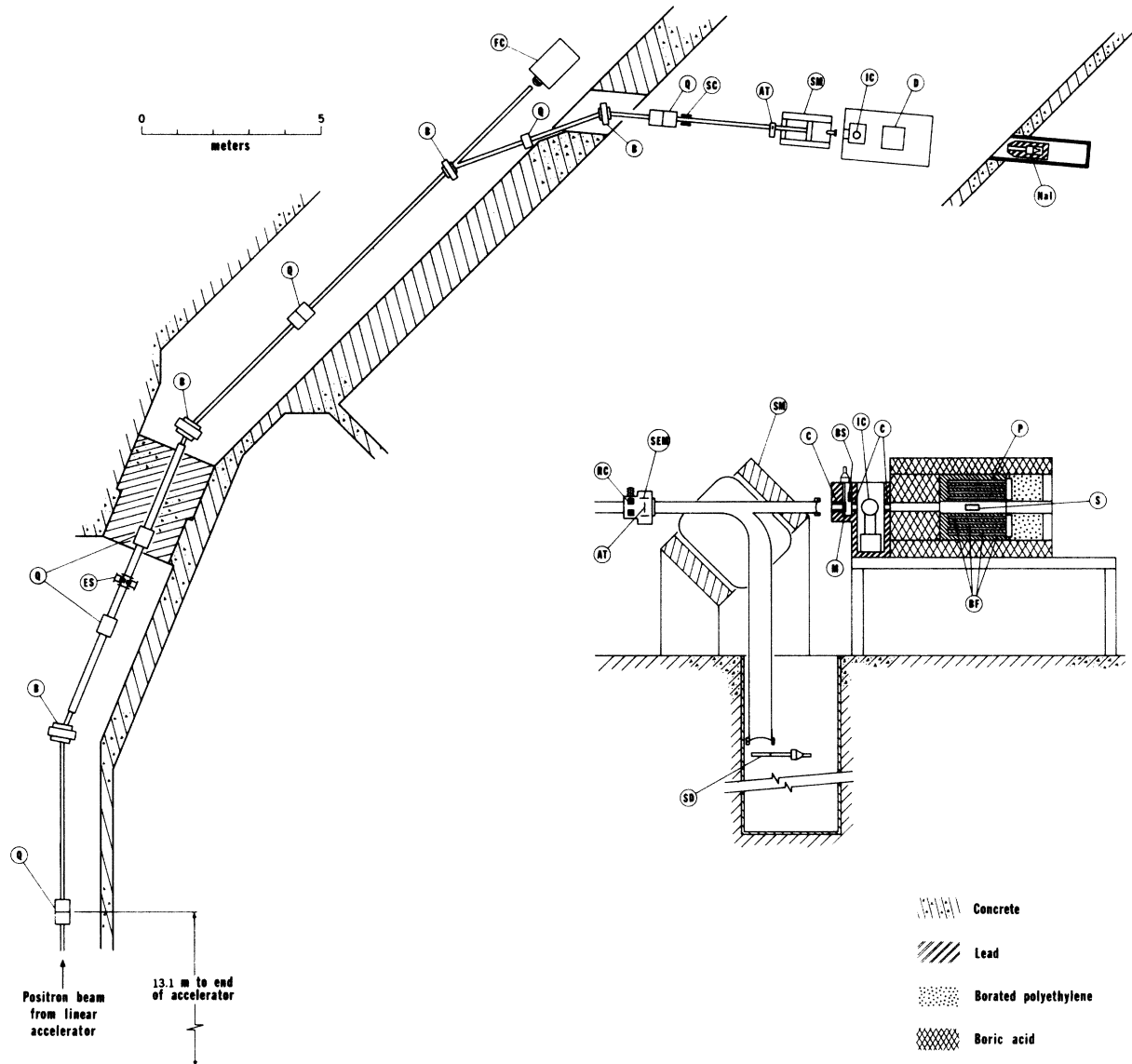

FIG. 1. Plan view of the beam transport system and experimental apparatus, with the latter shown in greater detail (in elevation view, in the inset). Indicated in the figure are: bending magnets, B; quadrupoles, Q; steering coils, SC; the annihilation target, AT; the sweeping magnet, SM; fixed and retractable collimators, C (nickel and heavimet) and RC (copper); scintillation detector monitors, M and SD, used in tuning the beam; the transmission ion chamber monitor, IC; the target sample, S; the neutron detector, D, consisting of BF_3 tubes, BF, embedded in a paraffin cube, P; and the photon spectrometer, NaI, used in the beam-monitor calibration measurements.

course, since our detector gives no information as to whether a proton is emitted along with a neutron, the (γ, n) cross section includes the (γ, pn) cross section and the $(\gamma, 2n)$ includes $(\gamma, p2n)$ etc., above the relevant thresholds. The thresholds of interest, taken from the tabulations of Wapstra and Gove,[14] are listed in Table I.

The photon energy resolution in annihilation-photon experiments depends on the energy spread in the incident positron beam, the degree of collimation of the forward-going photons, and the thickness of the annihilation target. The last has two effects: energy-loss straggling before annihilation occurs; and multiple scattering, which effectively broadens the angular acceptance of the collimators. These effects are described in some detail elsewhere.[15] In the present experiment the incident e^+ energy spread was about 0.4% full width at half-maximum (FWHM), which, together with the annihilation target thickness of 0.013 cm, resulted in an over-all photon energy resolution (FWHM) of about 75 keV at 10 MeV and 160 keV at 35 MeV. However, the dominant factor in terms of observing structural details in the cross section over much of the measured region is the point spacing, 120–200 keV over most of the range, imposed by running time limitations.

The energy calibration of the positron beam, *i.e.*, of the beam transport system, has been determined primarily from measurements of the (γ, n) yields over the 17.28-MeV peak in ^{16}O, the absolute energy of which is known accurately from neutron time-of-flight measurements.[16] The magnetic field in the energy-defining magnet was set and monitored by the use of a rotating-coil gaussmeter which is believed to be accurate to better than 0.1%.

III. EXPERIMENTAL RESULTS

Our measured cross sections for ^{58}Ni and ^{60}Ni are shown in Figs. 2 and 3, respectively. Values for the integrated cross sections are given in

TABLE I. Some particle emission thresholds for ^{58}Ni and ^{60}Ni (from Ref. 14) in MeV.

Reaction	^{58}Ni	^{60}Ni
(γ, n)	12.203 ± 0.008	11.388 ± 0.002
(γ, pn)	19.555 ± 0.004	19.993 ± 0.004
$(\gamma, 2n)$	22.470 ± 0.011	20.388 ± 0.002
$(\gamma, p2n)$	29.655 ± 0.004	28.565 ± 0.003
$(\gamma, 3n)$	$\cdots$	32.591 ± 0.008
$(\gamma, n2p)$	25.407 ± 0.004	26.945 ± 0.003
(γ, p)	8.177 ± 0.003	9.533 ± 0.002
$(\gamma, 2p)$	14.204 ± 0.003	16.903 ± 0.003

Table II. The ^{58}Ni total cross section exhibits considerable structure which persists well above 20 MeV; in fact, structure which is remarkably sharp for so heavy a nucleus at so high an excitation energy appears in the ^{58}Ni cross section between 22 and 26 MeV. The cross section reaches a maximum value of 27 mb at about 17.3 MeV. The envelope of giant-resonance states is rather broad, in agreement with previous experiments, and appreciable cross section remains at 33.5 MeV. The $(\gamma, 2n)$ cross section is very small throughout the measured energy range (and appears to be inhibited for about half an MeV above threshold); yet there is some indication of structure. In particular, there seem to be broad bumps
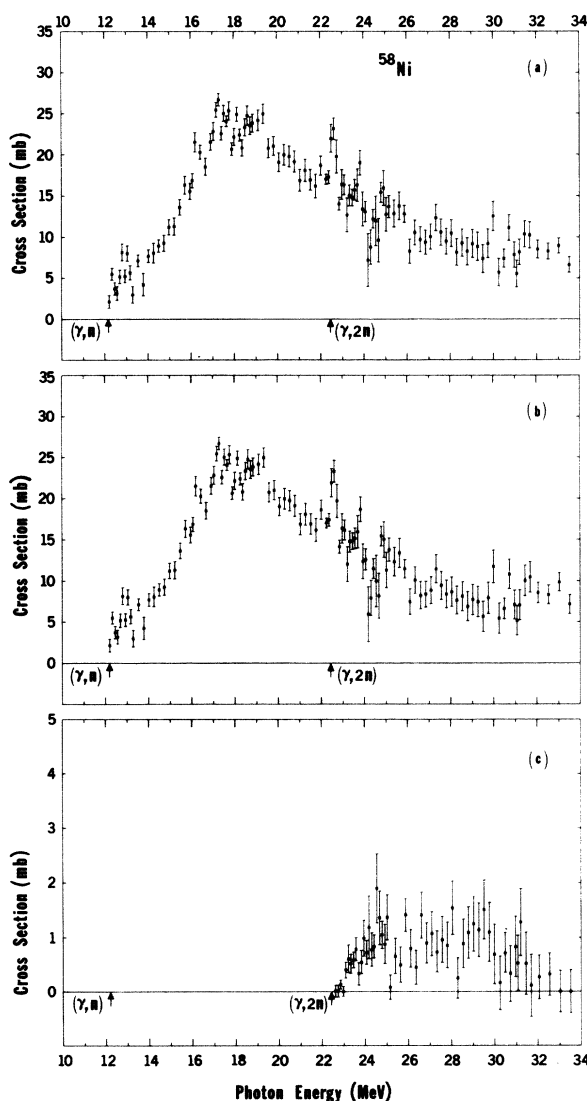
FIG. 2. Measured photoneutron cross sections for ^{58}Ni: (a) $\sigma(\gamma, Sn)$ (see Ref. 17); (b) $\sigma[(\gamma, n) + (\gamma, pn)]$; (c) $\sigma(\gamma, 2n)$.

in the $(\gamma, 2n)$ cross section at approximately 24 and 29 MeV.

In ^{60}Ni one sees, again, a rather broad giant resonance with evidence of considerable structure, though not nearly so pronounced as in the case of ^{58}Ni. The peak cross section of approximately 74 mb occurs at about 16.3 MeV. The $(\gamma, 2n)$ cross section is considerably more prominent than was the case for ^{58}Ni, both in absolute magnitude and in terms of the fraction of the total integrated cross section. Our statistics for ^{60}Ni are sufficiently good that a great deal of structure can be discerned in the $(\gamma, 2n)$ cross section, on both the leading and trailing edges of the main peak (which occurs in the vicinity of 24 MeV), in particular at 27, 28, and 31 MeV. No real $(\gamma, 3n)$ events were
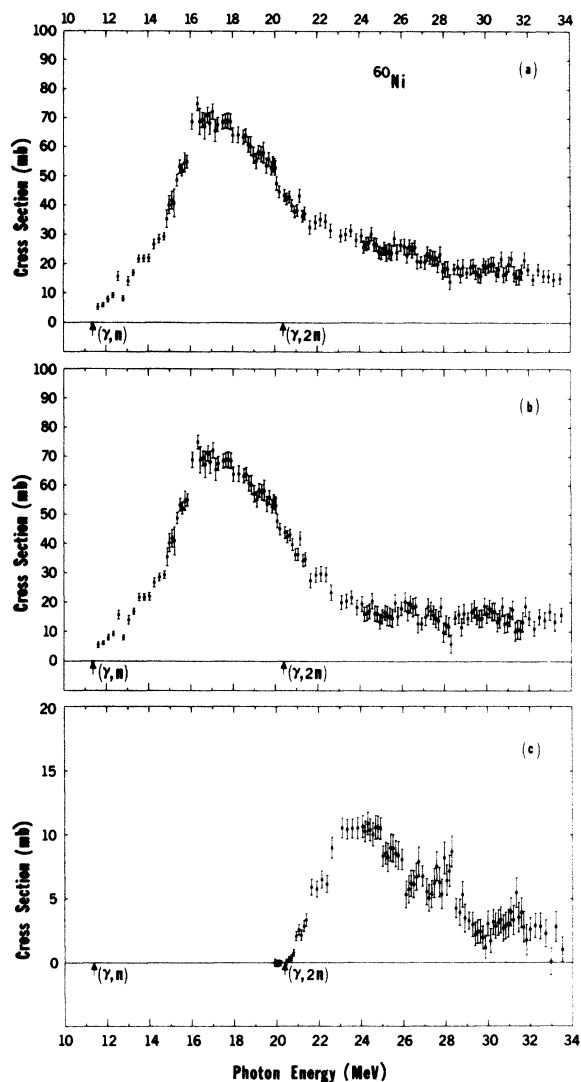
seen in these measurements.

Energies at which apparent structure (peaks or well-defined shoulders) exists in the cross sections are listed in Table III.

Finally, we note that unlike the case for heavier nuclei, the $[(\gamma, n) + (\gamma, pn)]$ cross sections remain dominant up to the highest energies measured, many MeV above the $(\gamma, 2n)$ thresholds.

The error bars shown on the data in Figs. 2 and 3 are statistical only. In addition to the random statistical errors there are three dominant sources of systematic error which introduce energy-dependent uncertainties into the results:

(1) There is at most a 4% uncertainty in the normalization factor used in subtracting the bremsstrahlung contribution to the counting rates. (The normalization factor accounts for differences in ion chamber response to a pure bremsstrahlung spectrum and a bremsstrahlung-plus-annihilation photon spectrum.) This uncertainty contributes negligible error to the cross sections near the thresholds where the subtraction is very small but becomes increasingly important at the higher energies. It results in an uncertainty of about 5% in the cross sections at the peak of the giant resonance and as much as 30% in the single-neutron cross sections above 30 MeV.

(2) There is an uncertainty in the annihilation-photon flux calibration which amounts to approximately 5% in the region of the giant resonance and below, but which could be as great as 10%

FIG. 3. Measured photoneutron cross sections for ^{60}Ni: (a) $\sigma(\gamma, Sn)$ (see Ref. 17); (b) $\sigma[(\gamma, n) + (\gamma, pn)]$; (c) $\sigma(\gamma, 2n)$.

TABLE II. Integrated photoneutron cross sections and related quantities from the data of the present experiment. The definitions used in this table are

$$\sigma_{int} \equiv \int_{E_{thr}}^{E_\gamma \ max} \sigma \, dE_\gamma \, , \qquad \sigma_{-k} \equiv \int_{E_{thr}}^{E_\gamma \ max} E_\gamma^{-k} \sigma \, dE_\gamma \, ,$$

where E_{thr} is the threshold energy (see Table I) and E_γ is the photon energy; the quantity (γ, Sn) is defined in Ref. 17. Errors on the integrated cross sections are dominated by the systematic errors as discussed in Sec. III of the text.

	^{58}Ni		^{60}Ni	
$E_\gamma \ max$	33.5	MeV	33.5	MeV
$\sigma_{int}(\gamma, Sn)$	286	MeV mb	704	MeV mb
$\sigma_{int}(\gamma, 2n)$	7.65	MeV mb	72.2	MeV mb
$\sigma_{int}[(\gamma, n) + (\gamma, pn)]$ [a]	278	MeV mb	632	MeV mb
$\sigma_{int}(\gamma, 2n)/\sigma_{int}(\gamma, Sn)$	0.027		0.103	
$\sigma_{-1}(\gamma, Sn)$	13.8	mb	35.6	mb
$\sigma_{-2}(\gamma, Sn)$	0.700	mb MeV^{-1}	1.90	mb MeV^{-1}
$\sigma_{int}(\gamma, Sn)/60(NZ/A)$	0.329		0.786	

[a] This quantity was obtained by subtracting $\sigma_{int}(\gamma, 2n)$ from $\sigma_{int}(\gamma, Sn)$; direct integration of the single-photoneutron cross sections gave the same values to within 0.5%.

at 35 MeV.

(3) The neutron-detector-efficiency calibration could be in error by as much as 5% at very high or very low neutron energies, owing to the uncertainties in the intensities of the calibration sources (but is less than 1% at neutron energies of around 2 MeV). In addition, the generally poorer statistics on the ring ratios *far* above the giant resonance could add an uncertainty of about 15% to the assigned detector efficiency used in computing the cross sections, but less than 4% uncertainty to $\sigma_{int}(\gamma, Sn)$.[17]

All other systematic errors are believed to be much smaller than the statistical errors.

IV. DISCUSSION

A. Comparison with previous experiments

Shown in Fig. 4 are visual fits to our total photoneutron results and those of previous experiments[3,5,6] performed with separated-isotopic samples. The total photoneutron cross sections are those given by the authors, corrected above the $(\gamma, 2n)$ threshold for neutron multiplicities according to a statistical model. We note that the corrections applied by Min and White[5] are essentially in agreement with the magnitudes of our $(\gamma, 2n)$ cross sections, whereas both Owen

TABLE III. Energies (MeV) at which peaks appear in the (γ, Sn) cross sections of ^{58}Ni and ^{60}Ni. The energies listed are those at which peaks or shoulders exist in the cross section. Actual resonance energies might be slightly different.

Peak No. [a]	^{58}Ni	^{60}Ni
1	12.3	12.6
2	12.8	13.7
3	13.1	14.4
4	13.6	15.1
5	14.2	15.5
6	15.7	16.3
7	16.3	17.0
8	17.3	17.7
9	17.7	18.6
10	18.2	19.6
11	18.6	21.2
12	19.3	22.1
13	22.6	24.5
14	23.8	
15	24.9	
16	25.7	

[a] We have included in the tabulations only the more well-defined peaks (or shoulders). In addition there are possible broad peaks at approximately 20.7, 27.8, and 30.9 MeV in ^{58}Ni, and at 23.5, 26.1, 27.5, and 30.3 MeV in ^{60}Ni, but the data are not sufficiently detailed to make a more definitive judgment about these.

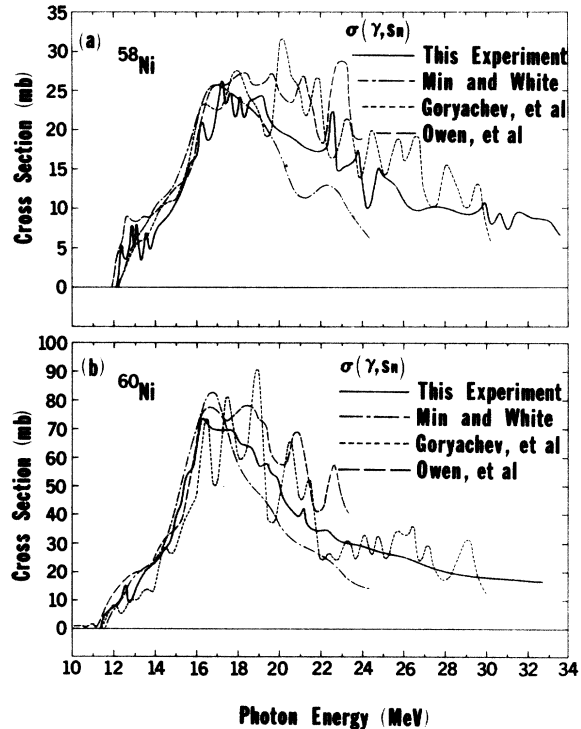FIG. 4. Comparison of the results of the present experiment for $\sigma(\gamma, Sn)$ with those of previous experiments for ^{58}Ni (a) and ^{60}Ni (b). Results of the present measurement are indicated by a solid line, those of Ref. 3 by a dashed line, those of Ref. 6 by a dotted line, and those of Ref. 5 by a dash-dot line.

et al.[3] and Goryachev *et al.*[6] appear to overestimate the two-neutron cross section. In particular the latter authors obtain resulting single-neutron cross sections which vanish above 27 MeV, while our results indicate that the single-neutron cross section of both isotopes furnishes at least half the strength up to the highest energy measured, and nearly all of the strength at the maximum energy (33.5 MeV).

Integrated cross sections obtained in the present work are compared with those from previous experiments in Table IV.

It can be seen in Fig. 4 that the low-resolution

TABLE IV. Comparison of integrated total photoneutron cross sections $\sigma_{int}(\gamma, Sn)$ with those from previous experiments.

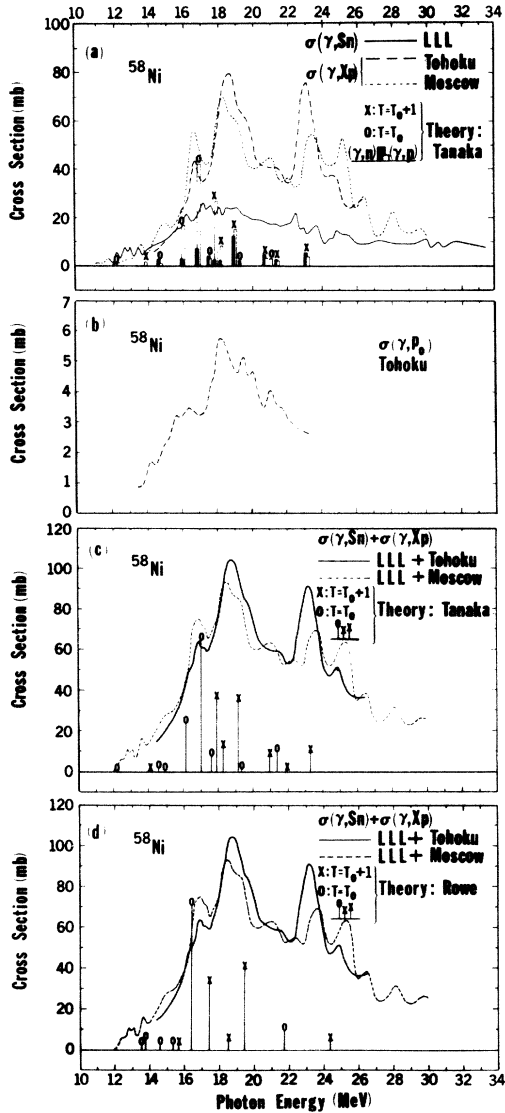| Reference	$E_{\gamma max}$ (MeV)	^{58}Ni (MeV mb)	^{60}Ni (MeV mb)
This experiment	30	256	643
Ref. 6 (Moscow)	30	310	620
This experiment	25	204	537
Ref. 5 (Virginia)	25	185	482

FIG. 5. Comparison of photoneutron and photoproton cross sections, and of experimental cross sections with (arbitrarily normalized) theoretical calculations for ^{58}Ni. (a) $\sigma(\gamma, Sn)$ and (γ, Xp) experimental cross sections compared with the theoretical results of Tanaka. The present results are represented by the solid line, those of Ref. 7 by the dotted line, and those of Ref. 8 by the dashed line. The theoretical prediction (Ref. 2) for photoneutron production is represented by the solid bars and for photoproton production by the open bars. Transitions to $T^>$ states and $T^<$ states are indicated by the symbols X and 0, respectively. (b) The value of $\sigma(\gamma, p_0)$ obtained from the data of Ref. 8 by multiplying the measured 90° differential cross section by 4π. (c) Total photon absorption cross sections obtained by adding the (γ, Sn) cross sections of the present experiment to the (γ, Xp) cross sections of Ref. 8 (solid line) and Ref. 7 (dotted line). The theoretical results of Ref. 2 for total photon absorption to $T^>$ and $T^<$ states are also shown. (d) Comparison of experimental total photon absorption cross sections with the theoretical calculation of Ref. 20.

data of Min and White generally agree qualitatively with the gross structure which we observe but fall considerably below our data above 18 MeV. Goryachev *et al.* and Owen *et al.*, on the other hand,
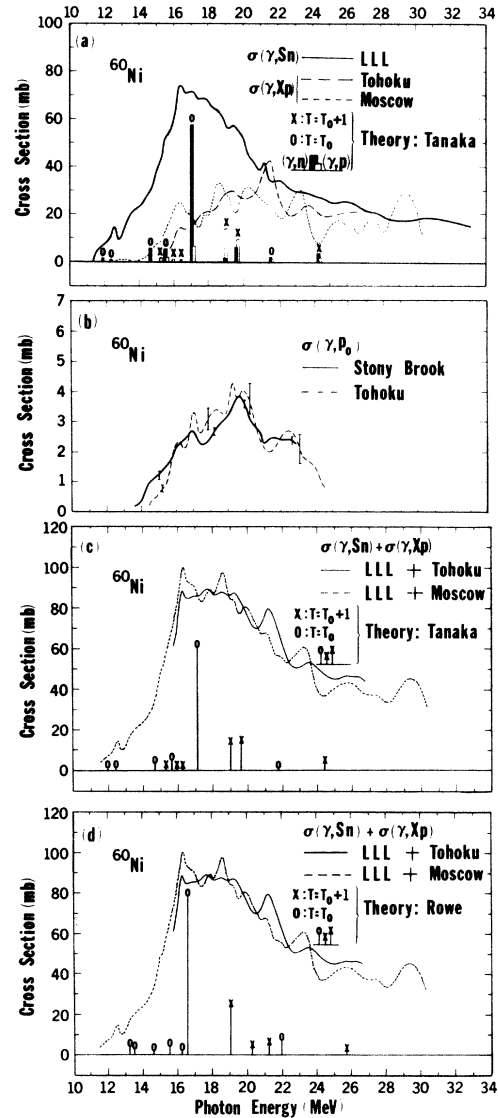

FIG. 6. Comparison of photoneutron and photoproton cross sections, and of experimental cross sections with (arbitrarily normalized) theoretical calculations, for ^{60}Ni. (a) $\sigma(\gamma, Sn)$ and $\sigma(\gamma, Xp)$ experimental cross sections compared with the theoretical results of Tanaka. The conventions used are the same as for Fig. 5(a). (b) The value of $\sigma(\gamma, p_0)$ obtained from the experiments of Ref. 1 (solid line) and Ref. 8 (dashed line). In both cases the measured 90° differential cross section has been multiplied by 4π. (c) Comparison of the experimental total photon absorption cross section with the theoretical results of Ref. 2. The conventions are the same as in Fig. 5(c). (d) Comparison of experimental total photon absorption cross sections with the theoretical results of Ref. 20.

observe considerable structure in the ^{58}Ni cross section but do not agree in detail with each other or with the results reported here. Furthermore, the structure in ^{60}Ni observed by the Russian group is vastly more prominent than that observed by either Owen *et al.* or the present measurement.

All four experiments are in reasonably good agreement on the magnitudes of the peak cross sections. Our ^{58}Ni integrated cross section, up to 30 MeV, is somewhat smaller than the value obtained by Goryachev *et al.* (see Table IV); Owen *et al.* did not report values for the integrated cross sections.

A point of interest can be brought out by a comparison of our high-energy data with those of Carver and Turchinetz.[11] The latter obtain for ^{58}Ni, at 32 MeV, $\sigma[(\gamma,pn)+(\gamma,2n)]\simeq13$ mb and $\sigma(\gamma,n)\simeq5$ mb. Our $(\gamma,2n)$ cross section is essentially zero above 32 MeV. Thus the Carver and Turchinetz 32-MeV cross section can be interpreted as implying $\sigma[(\gamma,n)+(\gamma,pn)]\simeq18$ mb and $\sigma(\gamma,pn)/\sigma(\gamma,Sn)\simeq0.75$. Although our own result of $\sigma[(\gamma,n)+(\gamma,pn)]=8$ mb at 32 MeV is only about half of the Carver and Turchinetz value, one might infer that it is dominated by the (γ,pn) process, and that $\sigma(\gamma,pn)\gg\sigma(\gamma,n)$ above about 30 MeV.

B. Integrated cross sections

From the values shown in Table II, it is evident that our integrated total-photoneutron cross sections, up to $E_{\gamma\,max}=33.5$ MeV do not constitute the entire classical dipole sum-rule values of $60(NZ/A)$ MeV mb for either nickel isotope. One reason is that the (γ,p) reaction makes a major contribution to the total photon absorption cross section. In ^{58}Ni, in fact, it was shown by Carver and Turchinetz that the integrated (γ,p) cross section, up to 32 MeV, is over twice as large as that for (γ,n).

In Figs. 5(a) and 6(a) we show a comparison of the photoproton cross sections[7,8] with the photoneutron cross sections obtained in the present experiment, representing each set of data by a visually fitted continuous curve. For the photoproton cross sections we include the results of the Moscow State University group,[7] obtained with a bremsstrahlung beam, as well as those of the Tohoku University group,[8] derived from an $(e,e'p)$ measurement. Both experiments rely on bremsstrahlung unfolding methods, with the well-known associated difficulties. In particular the structure shown in such measurments must be viewed with great caution, as is illustrated by the comparison of photoneutron measurements shown in Fig. 4. In the case of ^{58}Ni, both photoproton experiments agree fairly well on the location, if not the magnitude, of peaks in the cross section, but there is little agreement in the case of ^{60}Ni. We feel that

the structure shown in the Tohoku results is probably the more accurate since an indirect check on their reliability can be made by comparing the ^{60}Ni(γ,p_0) cross section obtained in the same experiment[8] with that derived by the Stony Brook group[18] from ^{59}Co(p,γ_0) measurements. This comparison (between 90° differential cross sections) is shown in Fig. 6(b), and the agreement between the two measurements, in terms of both absolute cross section and intermediate structure, is seen to be quite good except for the very low-energy region. We show, for completeness, the Tohoku ^{58}Ni(γ,p_0) differential cross section[8] multiplied by 4π in Fig. 5(b). It is interesting to note that although the ^{58}Ni-(γ,Xp) peak cross section is roughly twice as large as that of ^{60}Ni, the disparity in the (γ,p_0) cross sections of the two isotopes is not so large.

In order to obtain the total photon absorption cross sections for the nickel isotopes we simply have summed the curves for (γ,Sn) and (γ,Xp) shown in Figs. 5(a) and 6(a). The two sets of resulting cross sections (corresponding to the different photoproton experiments) are shown in Figs. 5(c) and 6(c). It should be pointed out that these results are not quite the total absorption cross

TABLE V. Integrated total photon absorption cross sections and related quantities from the combined data of the present experiment and Ref. 7. The (γ,Xp) cross sections of Ref. 7 have been used rather than those of Ref. 8 because the former extend over a wider energy range; in their mutually inclusive energy range (see Figs. 5 and 6) the integrated cross sections from the two (γ,Xp) measurements agree to within 2% for ^{58}Ni and 10% for ^{60}Ni, the values derived from the data of Ref. 8 being the larger in both cases. The total photon absorption cross section $\sigma(\gamma,\text{total})$ is assumed to be equal to $\sigma(\gamma,Sn)+\sigma(\gamma,Xp)$; that is the photon scattering cross section is assumed to be negligible and double counting, owing to the presence of $\sigma(\gamma,pn)$ in both $\sigma(\gamma,Sn)$ and $\sigma(\gamma,Xp)$, is ignored. The latter effect is reasonably compensated for, however (see footnote a).

	^{58}Ni		^{60}Ni	
$E_{\gamma\,max}$	33.5	MeV [a]	33.5	MeV [a]
$\sigma_{int}(\gamma,\text{total})$	850	MeV mb	1025	MeV mb
$\sigma_{-1}(\gamma,\text{total})$	41.3	mb	48.7	mb
$\sigma_{-2}(\gamma,\text{total})$	2.09	mb MeV^{-1}	2.62	mb MeV^{-1}
$\sigma_{int}(\gamma,\text{total})/$ $(60NZ/A)$	0.98		1.10	
$\sigma_{-1}(\gamma,\text{total})/A^{4/3}$	0.18		0.21	
$\sigma_{-2}(\gamma,\text{total})/A^{5/3}$	0.002 64		0.002 86	

[a] The (γ,Xp) data extend only to 30.1 MeV for ^{58}Ni and 30.5 MeV for ^{60}Ni; above these energies we have used the (γ,Sn) cross section only. Since much of the high-energy cross section probably comes from the (γ,pn) process, the error introduced is probably small and might very well compensate for the double counting of the (γ,pn) cross section below 30 MeV.

sections, since, for example, both the (γ, Sn) and (γ, Xp) cross sections contain the (γ, pn) cross section. The latter, therefore, is counted twice, and we have previously pointed out that, at least in ^{58}Ni, it may constitute the dominant part of the high-energy cross section. We also note that in adding the photoproton and photoneutron results, no attempt was made to smooth the latter in order to match the generally poorer resolution of the former. The peak-to-valley ratios of the narrower structures seen in the combined cross sections should therefore not be taken very seriously.

The integrated total photon absorption cross sections, together with the energy-weighted-integrated cross sections σ_{-1} and σ_{-2} are shown in Table V. These numbers were obtained using the combined Lawrence Livermore Laboratory and Moscow State cross sections shown in Figs. 5(c) and 6(c). The latter were used rather than the Tohoku results, because they cover a larger energy range and differ little in integrated area in spite of some differences in structure.

From Figs. 5 and 6 it seems likely that additional cross section remains in both nickel isotopes. The implications this would have for the dipole sum rule is not clear, for we have as yet no way of knowing how much of the higher-energy cross section results from $E1$ absorption. It has in fact been suggested[1] that the structure observed around 22 MeV in ^{60}Ni may be due to an $E2$ giant resonance. Shell-model calculations[2,4,19,20] indicate that the electric dipole strength of both isotopes is concentrated below 25 MeV (see Figs. 5–7). One might invoke arguments based on the greater effective charge of protons for $E2$ absorption to explain the preponderance of (γ, pn) over $(\gamma, 2n)$ strength in ^{58}Ni. Whereas for $E1$ radiation the effective charge of protons and neutrons is roughly equal for nuclei with $N \simeq Z$, for $E2$ radiation the ratio of effective charges is[21]

$$\left(\frac{Q_p}{Q_n}\right)_{E2} = \frac{A^2}{Z}\left(1 - \frac{2}{A} + \frac{Z}{A^2}\right).$$

For ^{58}Ni, $(Q_p/Q_n)_{E2} = 117$, and for ^{60}Ni, $(Q_p/Q_n)_{E2} = 125$. Thus for $E2$ transitions proton emission is expected to be greatly enhanced. Furthermore above the (γ, pn) threshold, proton emission can be followed by the emission of a neutron. At fairly high energies then, the (γ, pn) process is likely to be the dominant manifestation of $E2$ photon absorption.

Other possible explanations of the relatively large (γ, pn) cross section could lie in isospin considerations (see next section) or in the emergence of the quasideuteron effect as the dominant high-energy photon absorption process. The quasideu-

teron model provides a mechanism which enhances the emission of high-energy photonucleons through the short-range interaction between pairs of nucleons in the nucleus. Levinger has shown[22] that the two-nucleon wave function in the nucleus is proportional to the deuteron wave function and that the quasideuteron cross section is proportional to the number of effective quasideuterons in the nucleus times the free-deuteron cross section σ_d:

$$\sigma_{qd} = 6.4(NZ/A)\sigma_d.$$

At 33.5 MeV, $\sigma_d = 0.27$ mb[23]; $\sigma_{qd}(^{58}\text{Ni}, 33.5 \text{ MeV})$ $\simeq 25$ mb and $\sigma_{qd}(^{60}\text{Ni}, 33.5 \text{ MeV}) \simeq 26$ mb. In neither case is our measured cross section at 33.5 MeV, even if composed entirely of $\sigma(\gamma, pn)$, as large as the quasideuteron prediction.

In Tables II and V we show values for energy-weighted integrated cross sections σ_{-1} and σ_{-2} using both the total photoneutron cross section $\sigma(\gamma, Sn)$ and the total photon absorption cross section $\sigma(\gamma, Sn) + \sigma(\gamma, Xp)$. Using a harmonic-oscillator shell model, one can derive the relation,[24] σ_{-1} $= 0.36A^{4/3}$ mb. Experimentally however, σ_{-1} $\lesssim 0.20A^{4/3}$ for a wide range of nuclei with $A > 50$ previously measured at Livermore and else-

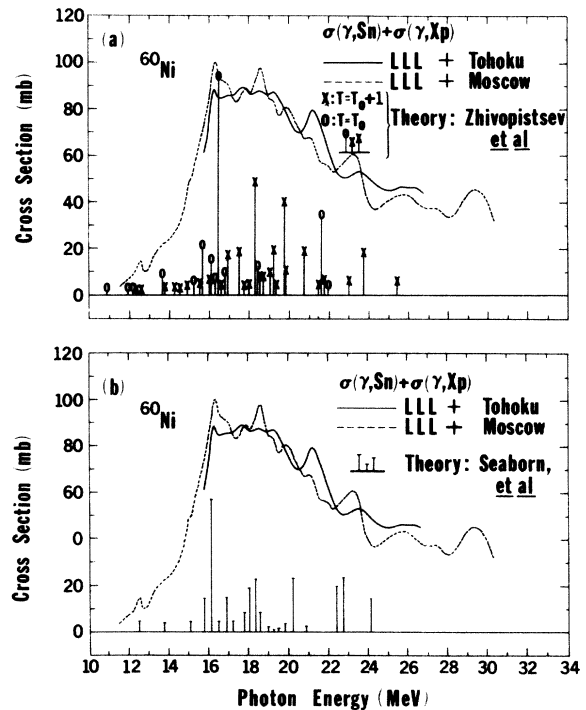FIG. 7. Comparison of experimental total photon absorption cross sections [see Fig. 6(c)] for ^{60}Ni with the results of (arbitrarily normalized) theoretical calculations: (a) Theoretical results from Ref. 19 for $T^>$ and $T^<$ states, X and 0, respectively; (b) Collective-correlations calculation from Ref. 4.

where.[25] The second moment of the cross section σ_{-2} is proportional to the nuclear polarizability and can be related to the nuclear symmetry energy K by the expression,[24] $\sigma_{-2} = 0.05175A^{5/3}/K$ mb MeV^{-1}, when K is in units of MeV.

In Table V we list values for $\sigma_{-1}/A^{4/3}$ and $\sigma_{-2}/A^{5/3}$ derived from the total photon absorption cross sections. For the former we find values quite close to 0.2, in agreement with previous experiments on other nuclei; from the values listed for the latter we can derive values for the symmetry energies of the nickel nuclei, $K = 19.6$ MeV for ^{58}Ni and 18.1 MeV for ^{60}Ni. These values agree quite well with the extrapolated A vs K relation derived from photonuclear measurements on heavier nuclei.[26]

C. Isospin effects

The $E1$ selection rules for a nucleus with ground-state isospin $T_0 \neq 0$ allow transitions to states with $T = T^< \equiv T_0$ and $T = T^> \equiv T_0 + 1$. It has been suggested that the existence of two sets of dipole states with different isospin can lead to gross structure, or "splitting," of the giant resonance since the $T^>$ states are predicted to lie at a higher energy than the $T^<$ states by an amount given by

$$\Delta E \equiv E(T^>) - E(T^<) = U_D(1 + T_0^{-1}),\tag{1}$$

where U_D is an effective symmetry energy for dipole states. The subject of isospin splitting of the giant resonance recently has been summarized by Akyüz and Fallieros,[27] who predict a value for the effective symmetry energy of

$$U_D \equiv \overline{V}(T_0/A) = 60(T_0/A) \text{ MeV}.\tag{2}$$

The present experimental situation with regard to isospin splitting of the giant resonance has been reviewed by Paul, Amann, and Snover[28]; they find, from an analysis of several experiments, empirical values of $\overline{V}$ ranging from 52 to 68 MeV for nuclei in the neighborhood of the nickel isotopes. Using $\overline{V} = 60$ MeV, the splittings predicted by Eq. (1) are 2.1 MeV for ^{58}Ni and 3.0 MeV for ^{60}Ni.

The ratio of the integrated cross section due to the $T^>$ states to that due to the $T^<$ states has been predicted by Fallieros and Goulard[29] to be approximately

$$\frac{I^>}{I^<} = \frac{T_0^{-1} - \frac{3}{2}A^{-2/3}}{1 + \frac{3}{2}A^{-2/3}}.\tag{3}$$

For the nickel isotopes Eq. (3) leads to the predictions $I^>/I^< = 0.8$ for ^{58}Ni ($T_0 = 1$) and $I^>/I^< = 0.36$ for ^{60}Ni ($T_0 = 2$). Then, although the energy split-

ting in ^{60}Ni is predicted to be greater than in ^{58}Ni, the fraction of strength in the $T^>$ states should be smaller, and it is not obvious in which isotope the splitting should be more apparent. Since there are other mechanisms which can lead to structure, or splitting, of the giant resonance (see next section), it is in fact not at all obvious that one can associate unambiguously a given peak in the photoneutron cross section with a given isospin, even where there is clearly resolved structure.

As a general rule, $T^<$ states in the $E1$ giant resonance decay preferentially via neutron emission since proton emission tends to be inhibited by the Coulomb barrier. For $T^>$ states, on the other hand, neutron decay to the $T = T_0 - \frac{1}{2}$ ground state of the daughter nucleus is inhibited by isospin conservation, and isospin-allowed proton decay should dominate if the states involved are good isospin eigenstates. According to this simple-minded picture the ratio of the (γ, p) to (γ, n) integrated cross sections would be given roughly by the ratio $I^>/I^<$ predicted by Eq. (3). Although this is approximately the case for ^{60}Ni, the (γ, p) mode is far more dominant in ^{58}Ni than the $I^>/I^<$ ratio would indicate; a probable explanation is embodied in the calculations of Refs. 2 and 20.

From a comparison of their ^{60}Ni (γ, p_0) cross sections with the (γ, n) data of Min and White,[5] Diener et al.[1] have concluded that the relative dominance of the (γ, p_0) cross section by the peak at 19.6 MeV together with the 16.5-MeV peak energy of the (γ, n) cross section is evidence for the predicted 3-MeV isospin splitting of the giant resonance. The present (γ, n) data show that the 19.6-MeV cross section is not as much smaller than that at the 16.5-MeV peak region, as the Min and White results indicate. Furthermore, although $\sigma(\gamma, Xp)$ as well as $(d\sigma/d\Omega)(\gamma, p_0)|_{90°}$ shows a peak at about 19 MeV, the Tohoku data[8] indicate a larger peak at 22 MeV.

We also note that even though shell-model calculations[2,19,20] tend to confirm the hypothesis that the strength in the 19-MeV region probably arises primarily from transitions to $T^>$ states, the (γ, Sn) cross section is still about a factor of 2 larger there than the (γ, Xp) cross section. It would therefore seem that there must still be considerable $T^<$ strength in this region unless most of the neutron decays occur via a $T = \frac{3}{2}$ excited state in ^{59}Ni (for example the isobaric analog of the ^{59}Co ground state); theoretical calculations[2,20] indicate that the latter decay mode may be preferred by at least some of the $T^>$ dipole states in ^{60}Ni, and the analagous decay mode might be dominant for some $T^>$ levels in ^{58}Ni. Experimentally we cannot determine to which states in the daughter nuclei the transitions occur.

D. Comparison with shell-model calculations

Theoretical calulations for both ^{58}Ni and ^{60}Ni have been performed by Tanaka[2] and by Ngo-Trong and Rowe.[20] Both calculations include excitations more complex than simple 1p-1h excitations and thus are able to keep the isospin of the excited dipole states a good quantum number.

Tanaka performed the calculation of photon absorption strength using three different types of forces. For the Serber-type force (referred to in Ref. 2 as "force 3") Tanaka also shows the results of a calculation of the $(\gamma, n)/(\gamma, p)$ branching ratios.[30] The latter are illustrated in Figs. 5(a) and 6(a), while the total absorption strengths computed with force 3 are shown in Figs. 5(c) and 6(c). It should be noted that Tanaka's calculated dipole strengths, when summed, are about 50% larger than the classical dipole sum rule.[2]

From Figs. 5 and 6 we infer that, for both isotopes, inclusion of the $T^>$ states in the calculation can explain the presence of some of the experimentally observed strength above the main peak of the giant resonance. Also the prominent features of the structure can be accounted for fairly well by Tanaka's calculation. Although there are some differences in the distributions of the calculated total absorption strengths between the different types of forces, we have shown the results only of force 3, since that is the only case for which the branching ratios were given in Ref. 2.

The results of Ngo-Trong and Rowe[20] are shown in Figs. 5(d) and 6(d); they are qualitatively similar to the results of Tanaka. As in the case of Tanaka's calculation, the summed dipole strengths of Ngo-Trong and Rowe exceed the predictions of the classical dipole sum rule, though by not quite so large an amount. In addition to the $T^>$ and $T^<$ dipole strengths, Ngo-Trong and Rowe have calculated (γ, n) and (γ, p) cross sections using an R-matrix approach. Although the predicted peak cross sections are too large to be considered in agreement with the measured values, the predicted ratios, like those calculated in Ref. 2, are able to explain the relative dominance of the (γ, p) cross section in ^{58}Ni and the (γ, n) cross section in ^{60}Ni. Since these results are similar to those of Ref. 2 [shown in Figs. 5(a) and 6(a)] we have not included them in the figures.

Calculations also have been performed for giant-resonance photon absorption in ^{60}Ni by Zhivopistsev et al.[19] and by Seaborn et al.[4] The former group have investigated the effect of coupling the simple particle-hole states to more complicated collective states, considering in particular, the role of two-particle–two-hole states. They find that both the $T^>$ and $T^<$ dipole states of ^{60}Ni are split by this coupling, leading to a rather rich intermediate structure as shown in Fig. 7(a). Zhivopistsev et al. have chosen the strength of the particle-hole interaction potential so that their strongest dipole state would occur at approximately 19 MeV. Although an earlier experiment[6] showed the largest peak in the (γ, n) cross section to be at about that energy, the present experiment shows that the main peak occurs closer to 16.5 MeV. Ideally, the calculation should be repeated with a different value for the particle-hole interaction potential. The main effect, however, would be to shift the spectrum of dipole states downward in energy. In comparing the Zhivopistsev calculations with the measured cross sections in Fig. 7(a), therefore, we have simply shifted the former downward in energy by an arbitrary amount.

The results of the ^{60}Ni calculation by Seaborn et al.[4] are shown in Fig. 7(b). These authors have used a particle-hole calculation for the dipole states and a collective model to treat the nuclear surface vibrations. The coupling of the dipole states and surface vibrations disperses the dipole strength, as shown in Fig. 7(b), and can thereby account, at least qualitatively, for some of the experimentally observed intermediate structure. Unfortunately, the question of isospin in the giant resonance is not treated explicitly by Seaborn et al.

None of the theoretical calculations which have been performed for the nickel isotopes takes into account the continum nature of the giant dipole resonance and therefore gives no information about the widths of the dipole states. In addition they all fail to account for the considerable strength observed above 25 MeV.

SUMMARY

The (γ, n) and $(\gamma, 2n)$ cross sections of ^{58}Ni and ^{60}Ni have been measured, using separated isotopes and nearly monoenergetic photons, from threshold to 33.5 MeV. The results agree fairly well, in absolute magnitude, with previous measurements, but the observed structure differs considerably in detail. The observed photoneutron cross section for ^{58}Ni is anomalously small; it is less than half the value observed for ^{60}Ni. Theoretical calculations provide a semiquantitative explanation of some of the observed features of the giant-resonance region but do not account for the continuing fairly large cross section above 25 MeV.

ACKNOWLEDGMENTS

‡Work performed under the auspices of the U. S. Atomic Energy Commission; preliminary reports appear in Bull. Am. Phys. Soc. 17, 16 (1972), and *Proceedings of the International Conference on Photonuclear Reactions and Applications,* edited by B. L. Berman (Lawrence Livermore Laboratory, Livermore, 1973), pp. 549–552.

†Deceased.

[1] E. M. Diener, J. F. Amann, P. Paul, and S. L. Blatt, Phys. Rev. C 3, 2303 (1971).

[2] Y. Tanaka, Prog. Theoret. Phys. 46, 787 (1971).

[3] D. G. Owen, E. G. Muirhead, and B. M. Spicer, Nucl. Phys. A140, 523 (1970).

[4] J. B. Seaborn, D. Drechsel, H. Arenhövel, and W. Greiner, Phys. Lett. 23, 576 (1966).

[5] K. Min and T. A. White, Phys. Rev. Lett. 21, 1200 (1968).

[6] B. I. Goryachev, B. S. Ishkhanov, I. M. Kapitonov, I. M. Piskarev, V. G. Shevchenko, and O. P. Shevchenko, Yad. Fiz. 10, 252 (1969) [transl.: Sov. J. Nucl. Phys. 11, 141 (1970)].

[7] B. S. Ishkanov, I. M. Kapitonov, I. M. Piskarev, V. G. Shevchenko, and O. P. Shevchenko, Yad. Fiz. 11, 485 (1970) [transl.: Sov. J. Nucl. Phys. 11, 272 (1970)].

[8] K. Shoda, private communication; see also H. Miyase, S. Oikawa, A. Suzuki, J. Uegaki, T. Saito, M. Sugawara, and K. Shoda, in *Proceedings of the International Conference on Photonuclear Reactions and Applications, Asilomar, March, 1973,* edited by B. L. Berman (Lawrence Livermore Laboratory, Livermore, 1973), p. 553.

[9] I. S. Gul'karov, N. G. Afanas'ev, V. M. Khvastunov, N. G. Shevchenko, V. D. Afanas'ev, G. A. Savitskii, and A. A. Khomich, Yad. Fiz. 9, 478 (1969) [transl.: Sov. J. Nucl. Phys. 9, 274 (1969)].

[10] L. Katz, R. G. Baker, R. N. H. Haslam, and R. A. Douglas, Phys. Rev. 82, 271 (1951).

[11] J. H. Carver and W. Turchinetz, Proc. Phys. Soc. Lond. 73, 585 (1959).

[12] D. S. Fielder, K. Min, and W. D. Whitehead, Phys. Rev. 168, 1312 (1968); G. Baciu, G. C. Bonazzola, B. Minetti, C. Molino, L. Pasqualini, and G. Piragino, Nucl. Phys. 67, 178 (1965); J. M. Wyckoff, B. Ziegler, H. W. Koch, and R. Uhlig, Phys. Rev. 137, B576 (1965).

[13] B. L. Berman, J. T. Caldwell, R. R. Harvey, M. A. Kelly, R. L. Bramblett, and S. C. Fultz, Phys. Rev. 162, 1098 (1967); see also previous references described therein.

[14] A. H. Wapstra and N. B. Gove, Nucl. Data A9, 303 (1971).

[15] C. P. Jupiter, N. E. Hansen, R. E. Shafer, and S. C. Fultz, Phys. Rev. 121, 866 (1961); C. R. Hatcher, R. L. Bramblett, N. E. Hansen, and S. C. Fultz, Nucl. Instrum. Methods 14, 337 (1961); R. L. Bramblett,

J. T. Caldwell, B. L. Berman, R. R. Harvey, and S. C. Fultz, Phys. Rev. 148, 1198 (1966).

[16] F. W. K. Firk, private communication.

[17] In our reaction notation we have essentially adopted the convention used by E. G. Fuller, H. M. Gerstenberg, H. Vander Molen, and T. C. Dunn, [*Photonuclear Reaction Data, 1973,* Natl. Bur. St. (U.S.) Special Publication No. 380 (U. S. GPO, Washington, D. C., 1973)], wherein (γ, Sn) represents the sum of all neutron-producing reactions, (γ, Xp) denotes total proton yield *etc.* We use (γ, pn) to represent either the (γ, np) or (γ, pn) reaction, since experimentally the two are indistinguishable.

[18] In Fig. 6b we have used the Stony Brook results (Ref. 1) averaged over 600-keV energy intervals for purposes of comparison with the moderate-resolution data of Ref. 8. In fact the inherent resolution of the Stony Brook data is much higher, and no fewer than 22 peaks are seen between 14- and 23-MeV excitation energies.

[19] F. A. Zhivopistsev, V. A. Lukashov, K. V. Shitikova, and N. P. Yudin, Czech, J. Phys. B22, 883 (1972); F. A. Zhivopistsev and K. F. Shitikova, Yad. Fiz. 16, 42 (1972) [transl.: Sov. J. Nucl. Phys. 16, 42 (1973)].

[20] C. Ngo-Trong and D. J. Rowe, Phys. Lett. 36B, 553 (1971); see also D. J. Rowe, *Proceedings of the International Conference on Photonuclear Reactions and Applications* (see Ref. 8), p. 717.

[21] See, *e.g.,* J. Eisenberg and W. Greiner, *Excitation Mechanisms of the Nucleus* (North-Holland, Amsterdam, 1970), p. 98.

[22] J. S. Levinger, Phys. Rev. 84, 43 (1951).

[23] B. Weissman and H. L. Schultz, Nucl. Phys. A174, 129 (1971).

[24] See, *e.g.,* J. S. Levinger, *Nuclear Photo-disintegration* (Oxford U. P., London, 1960), p. 50ff.

[25] E. G. Fuller, in *Proceedings of the International Conference on Photonuclear Reactions and Applications* (see Ref. 8), p. 1201.

[26] B. L. Berman, in *Proceedings of the International Conference on Photonuclear Reactions and Applications* (see Ref. 8), p. 569.

[27] R. Ö. Akyüz and S. Fallieros, Phys. Rev. Lett. 27, 1016 (1971).

[28] P. Paul, J. F. Amann, and K. A. Snover, Phys. Rev. Lett. 27, 1013 (1971); see also P. Paul in *Proceedings of the International Conference on Photonuclear Reactions and Applications* (see Ref. 8), p. 407.

[29] S. Fallieros and B. Goulard, Nucl. Phys. A147, 593 (1970).

[30] In Ref. 2 the decay of $T^{>}$ states is assumed to occur via the $T = T_0 + \frac{1}{2}$ isobaric analogs of the ground states of ^{57}Co and ^{59}Co.